



Chinese Society of Aeronautics and Astronautics
& Beihang University

Chinese Journal of Aeronautics

cja@buaa.edu.cn
www.sciencedirect.com



Effect of Martian atmosphere on aerodynamic performance of supersonic parachute two-body systems

Xiaopeng XUE^a, He JIA^b, Wei RONG^b, Qi WANG^b, Chih-yung WEN^{c,*}

^a School of Aeronautics and Astronautics, Central South University, Changsha 410083, China

^b Beijing Institute of Space Mechanics and Electricity, Beijing 100094, China

^c Department of Mechanical Engineering, The Hong Kong Polytechnic University, Hong Kong, China

Received 26 November 2020; revised 7 December 2020; accepted 28 December 2020

Available online 26 May 2021

KEYWORDS

Canopy flexibility;
Fluid structure interaction;
Martian atmosphere;
Supersonic parachute;
Unsteady flow

Abstract Supersonic flows around parachute two-body systems are numerically investigated by solving the compressible Navier-Stokes equations. In the present study, both rigid and flexible parachute models are considered, which comprise a capsule and a canopy. The objective of the present study is to investigate the effects of the Martian atmosphere on the unsteady flows produced by these parachute two-body models and the structural behavior of the flexible canopy. It was found that in the Martian atmosphere, the supersonic rigid parachutes with shorter trailing distances exhibited weaker aerodynamic interactions between the capsule wake and canopy shock, resulting in a smaller pressure distribution on the typical surfaces of the canopy. By contrast, because the flow modes around the flexible parachute in the Martian atmosphere were similar to those of the rigid parachute under the air conditions of the wind tunnel tests, the canopy shape was almost unchanged. When a new canopy material was designed by decreasing the Young's modulus and damping coefficient, an area oscillation phenomenon was observed in the flexible parachute with a trailing distance of 10 in the Martian atmosphere. Consequently, the Martian atmosphere (low density and pressure) has a significant effect on the aerodynamic performance of the flexible parachute system.

© 2021 Chinese Society of Aeronautics and Astronautics. Production and hosting by Elsevier Ltd. This is an open access article under the CC BY-NC-ND license (<http://creativecommons.org/licenses/by-nc-nd/4.0/>).

1. Introduction

On July 23, 2020, the first Chinese Mars lander, Tianwen-1, was successfully launched to Mars. To date, in successful Mars exploration missions, a supersonic parachute has always been deployed to decelerate the spacecraft during entry, descent, and landing on the Mars surface.¹ Supersonic decelerators for Mars entry missions have been investigated experimentally

* Corresponding author.

E-mail address: cymen@polyu.edu.hk (C.-y. WEN).

Peer review under responsibility of Editorial Committee of CJA.



since the late 1950s by the National Aeronautics and Space Administration (NASA).² Maynard³⁻⁴ first conducted an experiment to investigate the aerodynamic characteristics of ribbon parachute models under supersonic conditions, and observed that the drag coefficient of the parachute system depended significantly on the Mach number, canopy porosity, and distance between the forebody and canopy. In addition, the forebody wake had a marked effect on the drag performance of the parachute system. Subsequently, a series of wind tunnel and flight tests of various supersonic parachutes were conducted to select a suitable parachute for the Viking mission to Mars.⁵⁻⁸ A Disk-Gap-Band (DGB) parachute was found to be the best choice. It is worth mentioning that Maybue and Bobbitt⁵ performed a wind tunnel test of a DGB parachute, and found that the DGB parachute exhibited the oscillatory drag characteristics at supersonic speeds along with the low-frequency canopy breathing instability phenomenon. Moreover, this breathing instability became more severe as the Mach number increased from 2.0 to 3.0. In addition, it was observed that an increase in the trailing distance from the capsule and canopy resulted in an increase in the drag coefficient of the DGB parachute.⁵⁻⁸ However, in early experimental studies, very little was understood about the underlying mechanisms of the aerodynamic characteristics and performance of supersonic parachutes because of the complex dependent parameters. With advances in computer performance and numerical modeling techniques, the flow fields around the supersonic parachute systems can now be numerically investigated in detail.⁹⁻¹⁸ Recently, in the Mars Science Laboratory (MSL) mission to Mars, experimental and numerical investigations on the subscale MSL DGB parachute were conducted to qualify the largest DGB parachute from the Viking mission.^{10-12,19,20} The results indicated that the canopy breathing instability originated from the flow instability around the supersonic parachute, in which canopy-bow-shock/capsule-wake interactions were observed. In addition, it was found that this flow instability functionally depended on the Mach number, the relative size and proximity of the capsule to the canopy, Reynolds number, angle of attack, and material properties of the canopy.¹⁰⁻²⁰

However, it should be noted that to date most numerical and experimental studies have been performed in Earth's atmosphere because a Martian-like atmosphere is difficult to obtain in wind tunnel tests on the ground. Recently, a few numerical investigations^{21,22} on supersonic rigid and flexible parachute systems in a Martian atmosphere attempted to study the complex flow fields around parachute systems and their aerodynamic performance. It was observed that the flow mode around the supersonic rigid parachute was basically identical to that in Earth's atmosphere, and the stand-off distance of the capsule shock and the parachute drag forces were similar to those in air conditions for the rigid parachute system with different trailing distances. However, in contrast, the flexible parachute with the same material exhibited different deformation trends and corresponding drag coefficients in a Martian atmosphere than those in Earth's atmosphere.^{23,24} This study aims to investigate the complex flow fields and the aerodynamic interactions around the rigid and flexible parachutes numerically and comprehensively to understand the fabric dynamics of flexible parachutes in a Martian atmosphere.

2. Parachute models

Fig. 1 shows the supersonic parachute two-body system models used in the numerical simulations. The parachute two-body system consists of a capsule and a canopy. The canopy is hemispherical in shape with a diameter of D and a thickness of h , and the capsule is conical in shape with a frontal surface diameter of d and a half-angle of 20° . X is the axial distance from the frontal surface of the capsule to the inlet of the canopy. X/d is the trailing distance of the parachute, and d/D is the ratio of the diameter of the capsule to the diameter of the canopy.

In the rigid model, a solid rod with a diameter of d_1 is used to connect the capsule and canopy. Another solid rod with a diameter of d_2 is used to support the two-body system in the wind tunnel. This configuration is derived from the model employed in wind tunnel experiments at the Japan Aerospace Exploration Agency (JAXA).^{13,15,17} The flexible model is similar to a real parachute, except that there are no suspension lines. Note that these models are reproduced from the previous studies.^{13-15,17} to compare the flow physics and nonlinear change in the canopy shape in Earth and Martian atmospheres. As summarized in Table 1, the rigid model is used to simulate cases R1 and R2, and the flexible model is employed to simulate cases F1 and F2 in the present study.

In addition, it should be noted that in the flexible model cases, the thickness, h , of the canopy is zero in a geometrical sense,^{14,17} and the capsule is connected to the flexible canopy with suspension lines. Here, the suspension lines are only used to set up the force balance conditions, and the effect of these lines on the flow fields is not considered.^{14,17} In addition, the fabric porosity of the flexible canopy is also not taken into account in the present study.

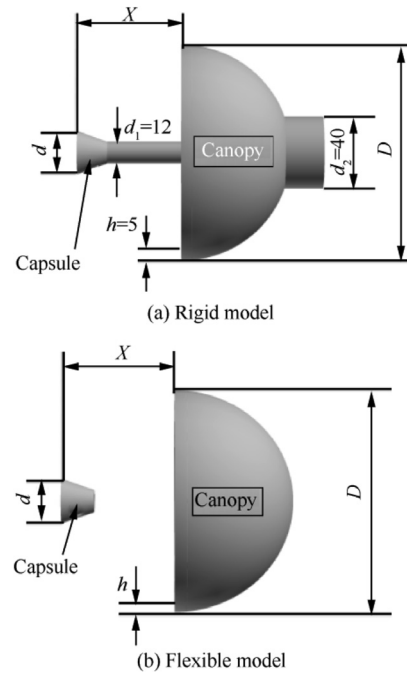


Fig. 1 Parachute two-body models used in this study (unit: mm).

Table 1 Specifications for simulation cases in the present study.

Case	X (mm)	d (mm)	D (mm)	X/d	d/D
R1, R2	57, 240	24, 24	120, 120	2.38, 10	0.2, 0.2
F1, F2	171, 240	24, 24	120, 120	7.13, 10	0.2, 0.2

3. Simulation methods

3.1. Computational conditions

As indicated in Table 2, Earth and Martian atmospheric conditions are used for both rigid and flexible simulation cases. Air atmospheric conditions at the wind tunnel of JAXA are employed for comparison with the Martian atmospheric conditions at $H = 1$ km and 7.1 km in the present study. Note that the Martian atmospheric conditions are calculated by²⁵

$$P_\infty = 0.669\exp(-0.00009H) \quad (1)$$

$$\rho_\infty = T_\infty/[0.1921(T_\infty + 273.1)] \quad (2)$$

$$T_\infty = 273.1 - 31 - 0.00098H \quad (H < 7 \text{ km}) \quad (3)$$

$$T_\infty = 273.1 - 23.4 - 0.00222H \quad (H \geq 7 \text{ km}) \quad (4)$$

where H is the height from the Martian surface, and P_∞, ρ_∞ , and T_∞ are the freestream pressure, density, and temperature, respectively. In addition, because the Martian atmosphere consists mainly of CO_2 , $\gamma = 1.3$ is employed for Martian environment cases; by contrast, $\gamma = 1.4$ is used for air atmosphere cases.

3.2. Flow calculation

Although the density is lower in the freestream conditions, especially for the Martian atmosphere, the Knudsen number is much lower than 10^{-3} . Thus, the working gas is approximated by a calorically perfect gas model. In the present calculations, Three-Dimensional (3D) rigid parachute systems (including R1 and R2) were simulated using an in-house, parallel, single-block, structured finite volume code, and the 3D compressible Navier-Stokes equations were computed to simulate the supersonic flow fields around the parachute two-body systems. Specifically, the Simple High-resolution Upwind Scheme (SHUS)²⁶ was employed to evaluate the inviscid fluxes, and the third-order Modified Upwind Scheme for Conservation Laws (MUSCL) with the Van Albada flux limiter was used to improve the accuracy of the SHUS. In addition, the usual second-order central differencing scheme was used to compute the viscous fluxes. For time integration of the accurate unsteady calculation, the third-order total variation

diminishing Runge-Kutta scheme was employed in the present study. Moreover, the initial conditions in the flow calculations utilized the freestream values listed in Table 2, while for the boundary conditions, no-slip and adiabatic conditions were imposed on the solid body surfaces. Note that the flow calculation methods based on Computational Fluid Dynamics (CFD) for the rigid parachute two-body systems were also applied to simulate the flexible parachute two-body systems (including cases F1 and F2).

In addition, in the flow calculations, the dimensionless time step, $t_1 = tV_\infty/D$ ^{13–15,17} (t is the dimensional time, V_∞ is the freestream velocity), was set to 1×10^{-5} for the rigid cases and 2×10^{-5} for the flexible cases to maintain a Courant-Friedrichs-Lewy number of less than 1 and facilitate comparison of the different cases.^{14,17}

Furthermore, no turbulence model was applied in the present calculations of rigid and flexible cases, because in the previous studies^{13–18,21,23} on both rigid and flexible parachute systems, the numerical results obtained by the laminar simulations were in good agreement with the experimental data in Refs. ^{13–18,21,23}. Thus, the same flow calculation methods and codes used previously^{13–18,21,23} were extended and applied here.

One of the features of the present calculation method is the use of the simple immersed boundary method^{14,16,17,23} to address the boundary conditions of the 3D flexible canopy in the flexible cases. In the previous studies^{14,16,17,23}, this method was successfully employed to describe the moving boundary of the flexible canopy surface. This method can approximately compute the velocity vectors of the virtual cells from the relationship between the fluid and virtual cells^{14,16,17,23}, as given by

$$\mathbf{V}_j = \mathbf{V}_{it} - \mathbf{V}_{in} + \mathbf{V}_w \quad (5)$$

$$\mathbf{V}_{it} = \mathbf{V}_i - \mathbf{V}_{in} \quad (6)$$

$$\mathbf{V}_{in} = (\mathbf{V}_i \mathbf{n}_j) \mathbf{n}_j \quad (7)$$

where \mathbf{V}_i and \mathbf{V}_j are the velocity vectors in the fluid and virtual cell, respectively; \mathbf{V}_w is the velocity of the flexible canopy; \mathbf{V}_{it} and \mathbf{V}_{in} are the tangential and normal components of the velocity, \mathbf{V}_i , respectively; \mathbf{n}_j is a unit vector normal to the flexible canopy surface. More details of the simple immersed boundary method can be found in Refs. ^{14,16,17,23}.

3.3. Structure calculation

In the present study, the Mass-Spring-Damper (MSD) model^{14,17,23} was employed to compute the structural dynamics of the flexible canopy for the flexible parachute-like cases. The flexible canopy material was assumed to be nylon^{14,17,23}, with a Young's modulus of 3 GPa and a density of 1150 kg/m³. In the MSD model, the canopy surface was considered as an assembly of mass nodes attached to springs and dampers,

Table 2 Air and Martian freestream conditions in this study.

Case	Ma_∞	P_∞ (Pa)	T_∞ (K)	ρ_∞ (kg/m ³)
Air	2.0	21,000	298	0.444
Mars1	2.0	369	234	0.0082
Mars2	2.0	639	241	0.0138

and its governing equations (Eq. (8)) were determined based on Newton's second law at each control node of the flexible canopy surface.^{14,17,23}

$$\frac{d^2 x_{ij}}{dt^2} = \frac{1}{m} \left\{ \sum_{k=1}^K (k_m \Delta l_k + c_m \frac{d(\Delta l_k)}{dt}) e_k - c_n (V_{ij} \cdot n_{ij}) n_{ij} + \Delta P_{i,j} + G_{i,j} + T_{i,j} \right\} \quad (8)$$

where m denotes the mass of a canopy node, and, k_m , c_m , and c_n denote the spring constant and tangential and normal damping coefficients, respectively. Note that the canopy material is highly nonlinear, and thus a larger spring constant than that of the linear Hook's law was suggested.^{17,27} The spring constant in this MSD model was $k_m = 4 \times 10^6$, which was obtained from the relationship between the Young's modulus and spring constant.^{17,23} Moreover, $c_m = 1 \times 10^{-1}$ and $c_n = 2 \times 10^{-4}$ were employed in the previous studies,^{14,17} where the reasonable results were demonstrated. In addition, l_k denotes the spring deformation value, e_k denotes the unit vector between two neighboring mass nodes, n_{ij} denotes the normal vector to the surface of the canopy, V_{ij} denotes the velocity of a mass node, $\Delta P_{i,j}$ denotes the pressure difference between the inner and outer surfaces of the canopy, and G_{ij} and T_{ij} denote the gravity force and the tension force of the suspension lines, respectively. Note that $K = 4$ for a typical interior mass node and $K = 3$ for a mass node at the canopy edge. In addition, the explicit second-order Runge-Kutta scheme was applied to compute the time variation of the flexible canopy shape in the flexible parachute-like cases.^{14,17,23}

3.4. Fluid-structure coupling calculation

In the calculation of flexible canopy cases, the weak coupling method was applied to solve the fluid and structure equations simultaneously. The coupling problem was separated into fluid and structural parts, and each part was solved in a serial manner.^{14,17} It was demonstrated that the mutual effect between the fluid and structural parts was rather sensitive in previous studies.^{14,17}

In the fluid and structural coupling calculation, the pressure distribution on the flexible canopy surface was computed from the flow calculation, and the pressure difference between the inner and outer surfaces of the flexible canopy was transferred to the structure calculation as the fluid force to obtain the displacement and velocity of each node of the canopy surface. Subsequently, these data were provided to the simple immersed boundary method to generate the new boundary conditions for the flow calculation at the next time step. More details can be found in Refs. 14,17,28. Note that no special forcing term was introduced into the original governing equations of the flow calculation. Here, the simple immersed boundary method works as a coupling method to combine the flow and structure calculation, which has demonstrated satisfactory results in previous studies.^{14,17,23,28}

3.5. Grids

Owing to the axisymmetric configuration of the parachute-like two-body system, the flow fields around the rigid and flexible parachute models were simulated using a structured grid with a single block, which was created based on a meridional

plane.^{13-18,21,23} 3D views of the grids and validity tests of the grid and temporal convergence were provided in Refs. 14,17,18. Thus, the details are omitted here. In this study, all the simulations were conducted using a similar grid density.

3.6. Validation of numerical methods

In previous numerical simulations of rigid and flexible parachutes,^{13-18,21,23,28} the simulation results of the R1 case (Table 1) under wind tunnel freestream conditions (Air in Table 2) were in good agreement with the results obtained from the JAXA wind tunnel tests.¹³⁻¹⁷ In addition, the simulation results of F1 under air freestream conditions were consistent with the experimental results in Ref. 29 and the drag performance of a real supersonic parachute.¹⁴ The flow and structure numerical methods employed in the above studies were also used for the calculation of rigid and flexible parachute-like models in the present study.

4. Results and discussion

4.1. Rigid parachute cases

In previous numerical simulations^{13,15-18} of rigid parachute models under wind tunnel conditions (Air condition), it was found that the most significant oscillation flow mode, the pulsation mode, occurs around the supersonic parachute two-body system with a short trailing distance, where the shock wave ahead of the capsule (capsule shock) exhibits a hemispherical shape, and periodically inflates and laterally expands in the radial direction. It was observed that the vortex ring at the foot of the shock wave ahead of the canopy (canopy shock) and the complex capsule-wake/canopy-shock and capsule-shock/canopy-shock interactions work together to drive the pulsation flow fields around the parachute two-body system.^{13,17,18}

Fig. 2 shows the instantaneous flow fields around the supersonic parachute-like system during a pulsation cycle in different atmospheres, indicating that the pulsation flow mode exists in both the Earth (Air conditions in Table 2) and Martian atmospheres. However, it can be seen that the capsule shock occurs closer to the capsule and becomes thinner in the Martian atmosphere. Fig. 3 shows a comparison of the variation in the ratio of the stand-off distance of the fore shock ahead of the capsule, s , to the diameter of the canopy, D , for Earth's and Martian atmospheres with non-dimensional time t_1 . These results indicate that there are minor differences between the time period and fluctuation amplitude of s/D during the pulsation mode. However, the stand-off distance is slightly smaller in the Martian atmosphere, as shown in Fig. 2. Furthermore, as Fig. 2 shows, the aerodynamic interactions in Martian atmosphere conditions become weaker, which causes that the pressure distribution on the canopy inner surface becomes much smaller in the Martian environments (Fig. 4(a)).

In previous studies under the Earth's atmosphere,^{15,18} as the trailing distance increases to $X/d = 10$, only the capsule wake interacts with the canopy shock. The interaction between the capsule shock and canopy shock seems to disappear because of the larger distance between the capsule and the canopy. As a consequence, the capsule shock shows no significant oscillation. This corresponds to the narrow capsule-

wake/canopy-shock interaction flow mode.^{15,18} The unsteady flow mode in the Martian atmosphere is consistent with that in the Earth's atmosphere. Thus, there are small differences

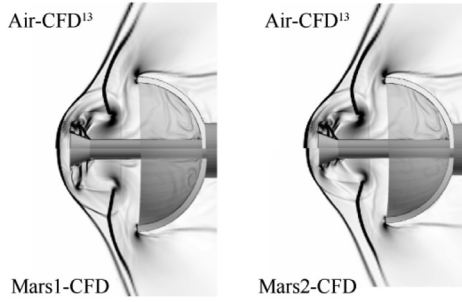


Fig. 2 Comparison of instantaneous flow fields around R1 rigid parachute system with $X/d = 2.38$ under different atmosphere conditions.

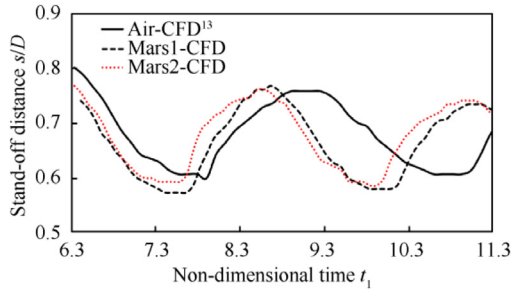


Fig. 3 Comparison of dimensionless stand-off distance for R1 rigid parachute system with $X/d = 2.38$ under different atmosphere conditions.

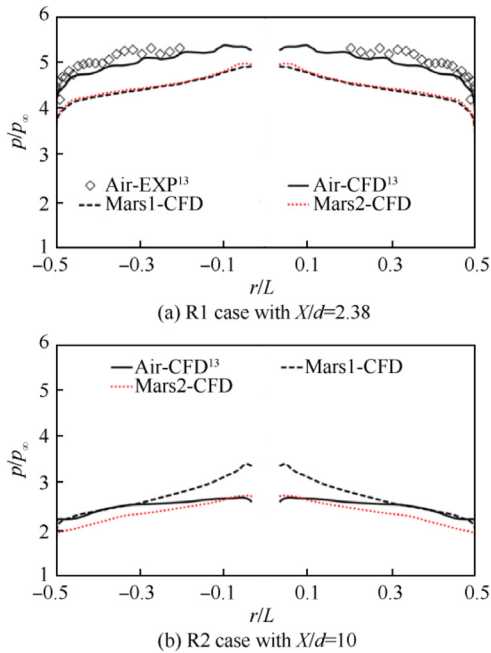


Fig. 4 Comparison of average pressure on the inner surfaces of supersonic rigid parachute systems under different atmosphere conditions.

in the pressure distributions on the inner surface of canopy under different atmospheres (Fig. 4(b)). Consequently, the Martian atmosphere has a greater effect on the performance of supersonic parachutes with shorter trailing distances. Moreover, it should be noted that there is a minor difference in the flow mode and corresponding pressure distribution on the typical surfaces of the canopy under Mars1 and Mars2 conditions. Thus, in the following simulations, the Mars2 condition is mainly employed to investigate the effect of the Martian atmosphere.

4.2. Flexible parachute cases

4.2.1. Original canopy material

In previous studies^{14,17,21,23} of flexible canopies with the same material as assumed above, it was observed that when the parachute system with $X/d = 7.13$ ($X = 171$ mm) was placed in the Earth's atmosphere (Air condition in Table 2), the shock ahead of the flexible canopy moved upstream of the canopy mouth and interacted with the narrow wake of the capsule, which resulted in the repeated pressure changes inside the canopy and corresponding oscillations in shape in the area.^{14,17} When X/d was increased to 10 ($X = 240$ mm, F2 case), a similar unsteady flow mode and shape change of the canopy was observed, as shown in Fig. 5(a).

It should be noted that in the unsteady flow mode, the strong flow instability generates significant unsteadiness in the drag force, which is computed from the pressure difference between the inside and outside of the canopy. Here the drag coefficient C_D was used as Eq. (9), instead of the drag force F_d .

$$C_D = \frac{F_d}{q \frac{1}{4} \pi D^2} \quad (9)$$

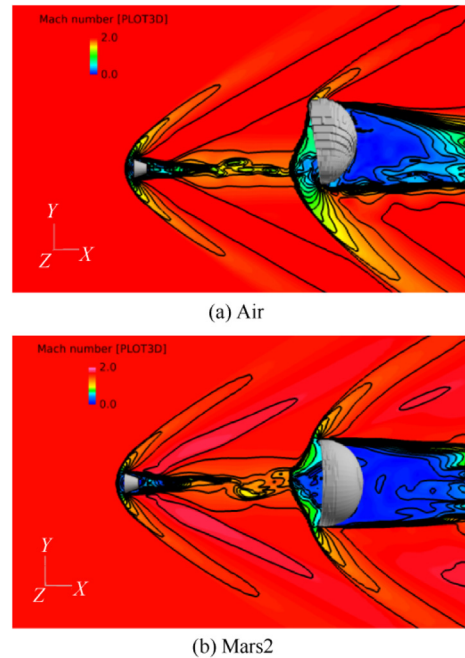


Fig. 5 Instantaneous flow fields around flexible parachute system with $X/d = 10$ under different atmospheric conditions.

$$q = \frac{\gamma}{2} P_{\infty} Ma_{\infty}^2 \quad (10)$$

where the dynamic pressure q is computed from the freestream pressure and freestream Mach number as shown in Eq. (10). This agrees with the method in Refs. 14, 17, 19.

In contrast, when the parachute system with $X/d = 7.13$ ($X = 171$ mm, F1 case) was placed in the Martian atmosphere (Mars2 condition in Table 2), the aerodynamic interaction of the capsule open wake and the canopy shock moved to the edge of canopy, and the canopy shock became much weaker, which resulted in a much smaller drag coefficient than that in the Air condition (Fig. 6).²¹ Note that the canopy shape was almost unchanged in the Martian atmosphere. As the trailing distance was increased to $X/d = 10$ ($X = 240$ mm, F2 case) in the Martian atmosphere (Mars2 condition in Table 2), a similar unsteady flow mode to that in the Earth's atmosphere was observed, as shown in Fig. 5(b); however, the canopy shape was almost unchanged (Fig. 5(b)). This does not conform to the real world, although the unchanged canopy

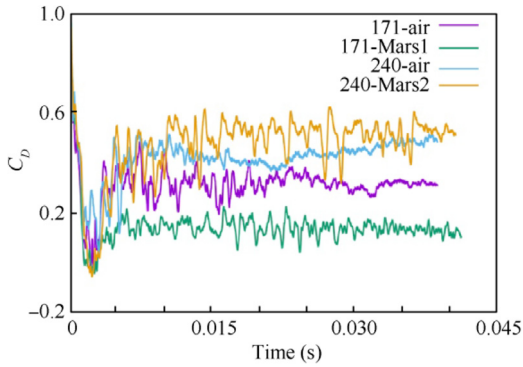


Fig. 6 Time histories of drag coefficients for different atmospheric cases; 171 denotes $X/d = 71.3$, and 240 denotes $X/d = 10$.

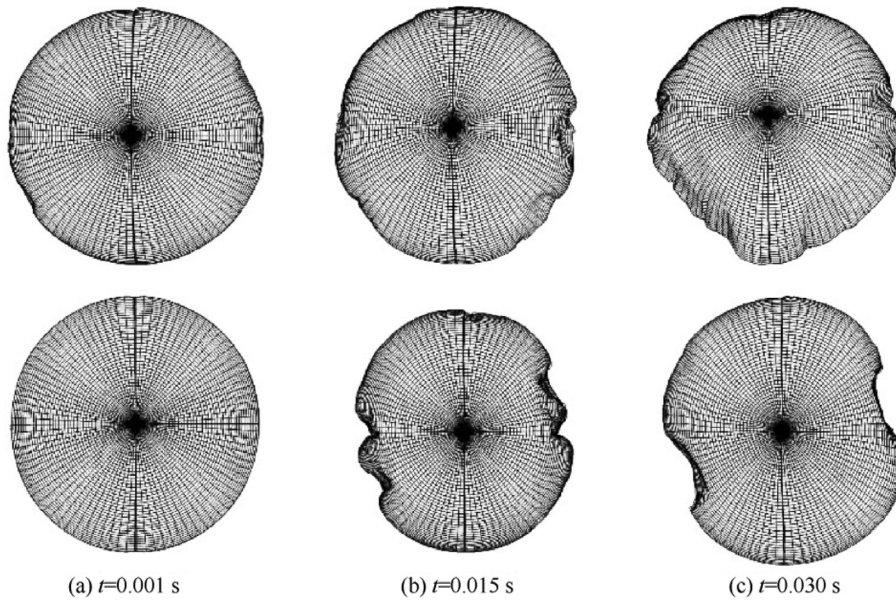


Fig. 7 Time variation of canopy shape for Air (upper) and Mars2 (lower) atmospheric conditions²³; the lower images employ the new parachute material.

resulted in a larger drag coefficient than that in other cases (Fig. 6).

Note that the performance of the flexible canopy with X/d of 7.13 and 10 in the Martian atmosphere (Mars 2 condition) is similar to the performance of the rigid canopy in the Earth's atmosphere,^{15,18} including the unsteady flow modes and almost unchanged canopy shape. This may be due to the lower density and pressure in the Martian atmosphere. Consequently, there is a large difference in the performance of the same canopy material in different atmospheres. A suitable canopy material for the Martian atmosphere will be investigated in the following section.

4.2.2. New canopy material

In order to improve the performance of the flexible canopy in the Martian atmosphere as mentioned above, a new material design of the parachute was considered here. A more flexible canopy material was designed, i.e., a lower Young's modulus (spring constant) and a lower damping coefficient of the canopy material were applied in the MSD model. The newly designed flexible parachute model was numerically applied to the flexible parachute with a trailing distance of 10, where the spring constant of the MSD model was decreased to $k_m = 1.5 \times 10^6$, and the normal and tangential damping coefficients were decreased to $c_m = 1.0 \times 10^{-3}$ and $c_n = 2.0 \times 10^{-5}$, respectively. As a result, the capsule wake became closed, aerodynamic interaction occurred between the capsule narrow wake and canopy shock, and a similar change in the canopy shape as that in the Air condition was observed (Fig. 7). Consequently, the drag coefficients of the new flexible canopy in the Martian atmosphere (Mars1 and Mars2 conditions) are similar to those in the Earth's atmosphere (Fig. 8). However, it should be noted that the amplitude of the fluctuation in the drag coefficient is much larger, which indicates that the effect of the flow instability related to the aerodynamic interaction between the capsule wake and canopy shock is

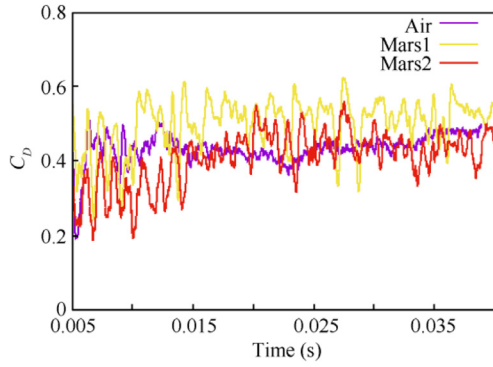
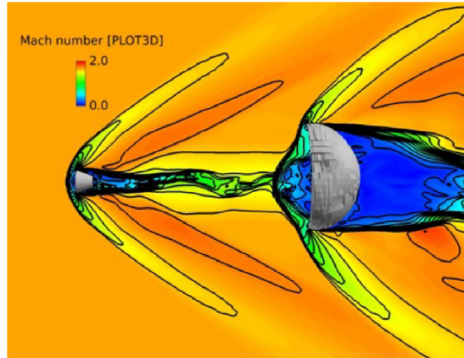


Fig. 8 Time histories of drag coefficients of flexible parachute with $X/d = 10$ under different atmospheric conditions.²³

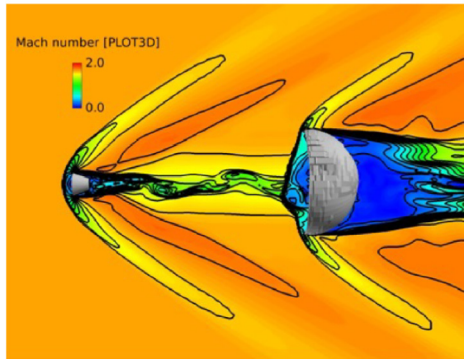
predominant, and further improvement of the canopy fabric flexibility is still needed.

4.2.3. Effect of canopy flexibility

In the present study, the new parachute system with $X/d = 10$ ($X = 240$ mm) was numerically simulated under the Air conditions at 30 km and Mars2 condition, and various canopy materials with different spring constants in the MSD model were applied to investigate the effect of the spring constant (from the Young’s modulus) on the performance of the flexible canopy. In addition, because the density and pressure of the Air condition at 30 km are similar to those of the Mars2 con-



(a) $k_m = 4 \times 10^5$



(b) $k_m = 3 \times 10^5$

Fig. 9 Instantaneous flow fields around flexible supersonic parachute system with $X/d = 10$ and different spring constants under the Martian atmosphere (Mars2 condition).

dition, the Air condition at 30 km was employed here to study the effects of atmospheric composition and the corresponding parameters on the performance of the flexible canopy. As a result, it was observed that the new canopies with various lower spring constants under the Air conditions at 30 km and Mars2 condition exhibited the same flow mode and similar changes in the canopy shape as the original canopy material under air conditions in the wind tunnel (Figs. 9 and 10). Compared with the results for the air conditions in the wind tunnel, the drag coefficients in lower density conditions, including 30 km in air and the Martian atmosphere, were slightly larger. Moreover, under both lower density and pressure conditions, there was a minor difference in the effects of the air at 30 km and Martian atmosphere on the flow mode and drag performance of the parachute systems. Note that, as shown in Fig. 6, the drag coefficient of the flexible canopy in the

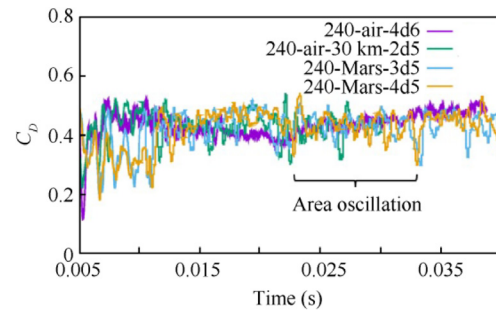
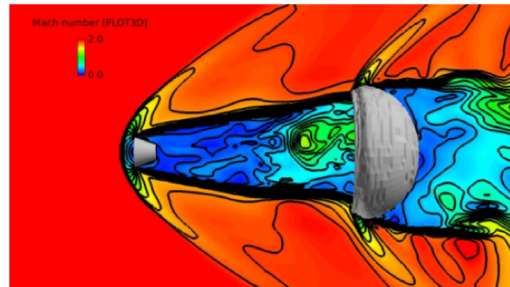
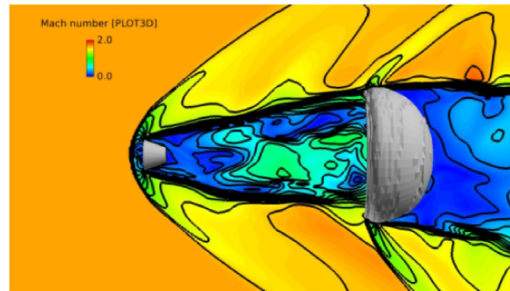


Fig. 10 Time histories of drag coefficients for flexible parachute with $X/d = 10$ ($X = 240$ mm) and various spring constants under different atmospheric conditions.



(a) Air condition at 30 km, $k_m = 2 \times 10^5$



(b) Mars2 condition, $k_m = 1 \times 10^5$

Fig. 11 Instantaneous flow fields around new flexible parachute system with $X/d = 7.13$.

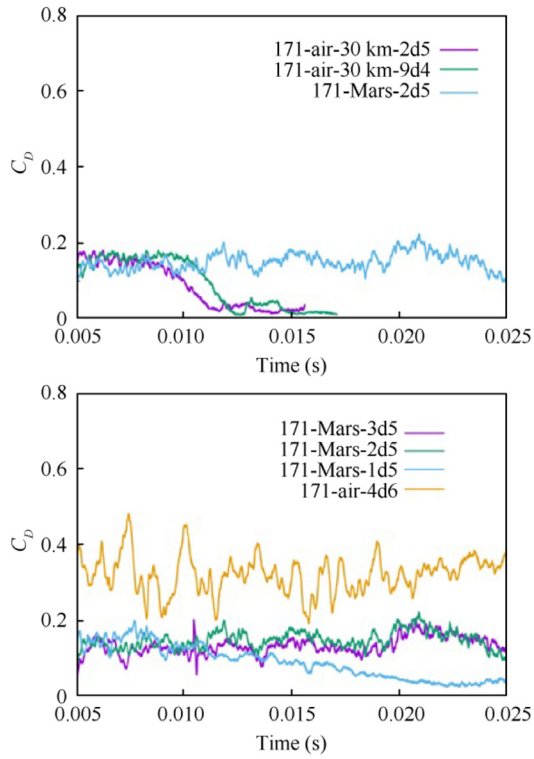


Fig. 12 Time histories of drag coefficients for new parachute with various spring constants under different atmospheric conditions.

Earth's atmosphere shows a significant large periodical change due to "area oscillation" and high-frequency change due to "flow instability", and the drag coefficient of the canopy in the Martian atmosphere shows the only high-frequency change due to "flow instability". As shown in Fig. 10, it is further confirmed that the drag coefficient arises from the pressure difference between the inside and outside of the canopy, which is significantly affected by two key factors: flow instability and the change in canopy shape. Periodical canopy "area oscillation" results in a periodical change in the drag coefficient.

However, when the parachute system with $X/d = 7.13$ ($X = 171$ mm) and the new canopy material was numerically investigated further under 30 km air and Martian conditions, it was observed that the flow mode under both atmospheric conditions was still the open canopy-wake/canopy-shock interaction, as shown in Fig. 11, indicating that the periodical changes in the canopy shape did not occur with the newly designed material. As shown in Fig. 12, compared with the canopy performance under air conditions in the wind tunnel, the drag coefficients in the lower density conditions including 30 km in air and the Martian atmosphere were much smaller, perhaps because the canopy with a lower Young's modulus becomes more flexible and shrinks easily and more rapidly. It should be noted that the drag coefficients under the air conditions at 30 km were very small and tended toward zero with time, indicating that the canopy shrinks quite significantly after 0.01 s.

To compare the drag performance of the flexible canopies with the original ($k_m = 4 \times 10^6$) and new (lower k_m) materials under different atmospheric conditions, Fast Fourier

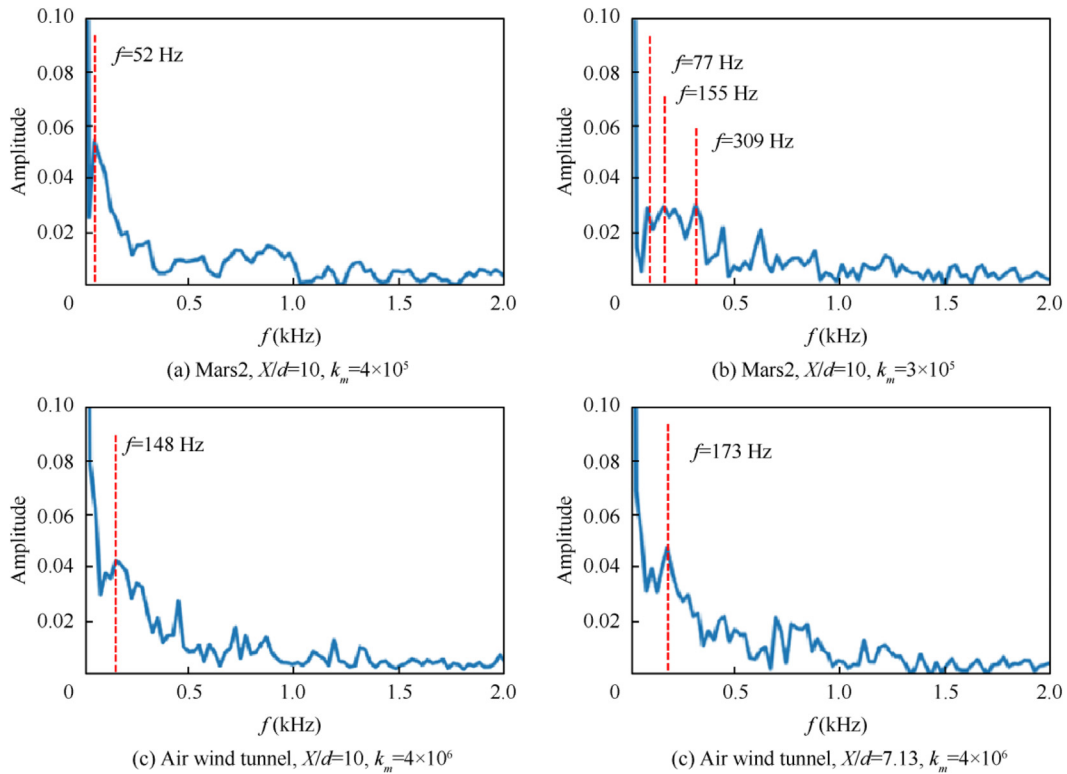


Fig. 13 FFT analysis of time variation in drag coefficients from Figs. 10 and 12.

Transform (FFT) analyses were conducted for the time variation in the drag coefficients, as shown in Fig. 13. It can be observed that for the F2 parachute model with $X/d = 10$, the lowest frequency (the largest time period) under Martian conditions is larger (smaller) than that under the air conditions of the wind tunnel. This indicates that in the Martian atmosphere, the canopy shape periodically changes over a smaller time period, and the flexibility of the canopy material is improved. In contrast, for F2 parachute model, when the spring constant k_m decreases from 4×10^5 to 3×10^5 in Martian atmosphere, the canopy material becomes more flexible, and the time period (lowest frequency) of canopy change becomes much smaller (larger). For the F1 parachute model with $X/d = 7.13$ in the wind tunnel air conditions, there are some complex fragmentary frequencies with the similar amplitude. This implies that the flow instability (the related frequency: 309 Hz) and/or the periodic canopy shape (the related frequency: 155 Hz and 77 Hz) change result in very strong variation in drag coefficient. A comparison between the F1 and F2 cases for $X/d = 7.13$ and 10 shows that much stronger variation in the drag coefficient occurs in the $X/d = 10$ cases, where the amplitudes are larger. On the other hand, much more unstable flow fields occur at $X/d = 7.13$, where a more complicated frequency distribution for the same amplitude is observed.

5. Conclusions

The supersonic flow over rigid and flexible parachute two-body models under different atmospheric conditions was numerically studied at a freestream Mach number of 2.0, and the effects of the Martian atmosphere on the flow behavior and fabric dynamics of the parachute two-body system were investigated numerically. The results obtained in this study can be summarized as follows:

- (1) In the Martian atmosphere, the unsteady flow modes around the supersonic rigid and flexible parachute two-body systems with larger trailing distance (i.e., $X/d = 10$) are identical to those in the Earth's atmosphere. However, the aerodynamic interactions around the parachute with short trailing distances (i.e., $X/d = 7.13$ and 2.38) become weaker, and the pressures on the typical surfaces of the parachute system decrease in the Martian atmosphere.
- (2) The Martian atmosphere (i.e., low density and pressure) has a significant effect on the aerodynamic performance of flexible parachute systems. Owing to the low density and pressure, the flow modes around the flexible parachutes with X/d of 7.13 or 10 and the same original canopy material (larger Young's modulus and damping coefficient, i.e., less flexibility) are similar to those of the rigid models under the air conditions of the wind tunnel, and an unchanged canopy shape is observed.
- (3) From the time variation of drag coefficient for the flexible canopies, it can be seen that the drag coefficient of the flexible canopy with less flexibility in the Martian atmosphere shows a high-frequency change due to "flow instability", which is similar with the performance of rigid models, while the drag coefficient of the less flexible canopy in the Earth's atmosphere or more flexible

canopy in the Martian atmosphere exhibits a significant large periodical change due to "area oscillation" and a high-frequency change due to "flow instability".

- (4) Under Martian atmosphere conditions, a reasonable canopy material was specially considered, and a smaller Young's modulus and damping coefficient of the canopy material were defined for the design of the canopy to improve its flexible ability. The area oscillation phenomenon and the corresponding drag performance were observed again for the newly designed canopy. In addition, it was also indicated that the drag performance was significantly affected by two key factors: flow instability and the periodical change in canopy shape. However, in the future studies, accurate characteristics of the flexible canopy material models and their effect mechanisms should be further investigated in the Martian atmosphere.

Declaration of Competing Interest

The authors declare that they have no known competing financial interests or personal relationships that could have appeared to influence the work reported in this paper.

Acknowledgements

This study was co-supported by the National Natural Science Foundation of China (Nos. 11702332 and 12072377) and the Natural Science Foundation of Hunan Province, China (No. 2018JJ3627).

References

1. Reynier P. Survey of aerodynamics and aerothermodynamics efforts carried out in the frame of Mars exploration projects. *Prog Aerosp Sci* 2014;70:1–27.
2. Sengupta A. Fluid structure interaction of parachutes in supersonic planetary entry 21st AIAA aerodynamic decelerator systems technology conference and seminar. Reston: AIAA; 2011. p. 1–12.
3. Maynard J. Aerodynamics of decelerators at supersonic speeds. *AIAA proceedings of the recovery of space vehicles symposium*. Reston: AIAA; 1960. p. 48–54.
4. Maynard J. Aerodynamic characteristics of parachute at Mach numbers from 1.6 to 3. Washington, D.C.: NASA; 1961. Report No.:TN-D-752.
5. Mayhue R, Bobbitt P. Drag characteristics of a Disk-Gap-Band parachute with a nominal diameter of 1.65 meters at Mach numbers from 2.0 to 3.0. Washington, D.C.: NASA; 1972. Report No.: TN-D-6894.
6. Steinberg SY, Siemers PM, Slayman RG. Development of the Viking parachute configuration by wind-tunnel investigation. *J Spacecraft Rocket* 1974;11:101–7.
7. Moog RD, Michel F. Balloon launched Viking decelerator test program summary report. Washington, D.C.: NASA; 1973. Report No.:TR-3720359.
8. Moog RD, Bendura RJ, Tlmons JD, et al. Qualification flight tests of the Viking decelerator system. *J Spacecraft Rockets* 1974;11(3):188–95.
9. Lingard S, Darley G. Simulation of parachute fluid structure interaction in supersonic flow 18th AIAA aerodynamic decelerator systems technology conference and semina. Reston: AIAA; 2005. p. 1–9.

10. Barnhardt M, Drayna T, Nompelis I, et al. Detached eddy simulations of the MSL parachute at supersonic conditions *19th AIAA aerodynamic decelerator systems technology conference and seminar*. Reston: AIAA; 2007. p. 1–11.
11. Gidzak V, Barnhardt M, Drayna T, et al. Comparison of fluid-structure interaction simulations of the MSL parachute with wind tunnel tests *20th AIAA aerodynamic decelerator systems technology conference and seminar*. Reston: AIAA; 2009. p. 1–12.
12. Karagiozis K, Kamakoti R, Cirak F, et al. A computational study of supersonic Disk-Gap-Band parachutes using large-eddy simulation coupled to a structural membrane. *J Fluids Struct* 2011;**27**(2):175–92.
13. Xue XP, Koyama H, Nakamura Y. Numerical simulation on supersonic aerodynamic interaction of a parachute system. *Trans JSASS Aerospace Tech Japan* 2013;**11**:33–42.
14. Xue X, Nakamura Y. Numerical simulation of a three-dimensional flexible parachute system under supersonic conditions. *Trans JSASS Aerospace Tech Japan* 2013;**11**:99–108.
15. Xue XP, Nishiyama Y, Nakamura Y, et al. Parametric study on aerodynamic interaction of supersonic parachute system. *AIAA J* 2015;**53**(9):2796–801.
16. Xue X-P, Koyama H, Nakamura Y, et al. Effects of suspension line on flow field around a supersonic parachute. *Aerosp Sci Technol* 2015;**43**:63–70.
17. Xue X, Nakamura Y, Mori K, et al. Numerical investigation of effects of angle-of-attack on a parachute-like two-body system. *Aerosp Sci Technol* 2017;**69**:370–86.
18. Xue X, Nishiyama Y, Nakamura Y, et al. High-speed unsteady flows past two-body configurations. *Chin J Aeronaut* 2018;**31**(1):54–64.
19. Sengupta A, Kelsch R, Roeder J, et al. Supersonic performance of disk-gap-band parachutes constrained to a 0-degree trim angle. *J Spacecraft Rockets* 2009;**46**(6):1155–63.
20. Sengupta A, Steltzner A, Witkowski A, et al. Findings from the supersonic qualification program of the Mars Science Laboratory parachute system *20th AIAA aerodynamic decelerator systems technology conference and seminar*. Reston: AIAA; 2009. p. 1–16.
21. Xue XP, Dai G. Effect of Martian atmosphere on aerodynamics interaction of a parachute system *The 9th across strait symposium on shock waves/complex flows*. p. 1–2.
22. Muppidi S, Farrell C, Tanner C, et al. Modeling and flight performance of supersonic disk-gap-band parachutes in slender body wakes *2018 atmospheric flight mechanics conference*. p. 1–19.
23. Xue XP, Wang Y, Zhao DJ, et al. Effect of Martian atmosphere on aerodynamic performance of a flexible supersonic parachute system *The 32nd international symposium on shock waves*. p. 1–2.
24. Huang D, Avery P, Farhat C, et al. Modeling, simulation and validation of supersonic parachute inflation dynamics during Mars landing *AIAA scitech 2020 forum*. Reston: AIAA; 2020. p. 1–21.
25. Grc.nasa.gov. NASA: Mars atmosphere model [Internet]. 2015 May 5 [cited 2020 Nov 26]. Available from: <https://www.grc.nasa.gov/www/k-12/airplane/atmosmrm.html>.
26. Shima E, Jounouchi T. Roe of CFD in aeronautical engineering (No.14) -AUSM type upwind schemes-. Proceedings of 13th NAL symposium on aircraft computational aerodynamics;1997. p. 41-6.
27. Kim J, Li Y, Li X. Simulation of parachute FSI using the front tracking method. *J Fluids Struct* 2013;**37**:100–19.
28. Tokunaga K, Takayangi H, Suzuki T, et al. Computational study of supersonic parachute on opening dynamics. *J Japan Soc Aeronaut Space Sci* 2017;**65**(5):208–14 [Japanese].
29. Reichenau D. Aerodynamic characteristics of disk-gap-band parachutes in the wake of Viking entry forebodies at Mach numbers from 0.2 to 2.6. Tennessee: Arnold Air Force Station, Arnold Engineering Development Center; 1972. Report No.: AEDC-TR-72-78.